Correlation and polarization effects in two-photon photoionization of Ar

I. D. Petrov* and B. M. Lagutin
Rostov State University of Transport Communications, 344038 Rostov-on-Don, Russia

V. L. Sukhorukov
Institute of Physics, Southern Federal University, 344090 Rostov-on-Don, Russia

A. Knie and A. Ehresmann
Institut für Physik, Universität Kassel, D-34132 Kassel, Germany
(Received 8 August 2015; revised manuscript received 8 January 2016; published 9 March 2016)

A method for the calculation of transition amplitudes of two-photon ionization processes is developed. It is based on computing a correlation function, which enables the summation over intermediate states of two-photon transitions. Two-photon ionization transition amplitudes were calculated in the lowest order of perturbation theory with taking into account many-electron correlations. The noniterative numerical scheme provided a solution of the differential equation for the correlation function at exciting-photon energies close to the intermediate discrete resonance states. Cross section and angular distribution parameters for photoelectrons of the two-photon $3p$ photoionization of Ar were calculated. The exciting-photon energy ranged from 8 eV to 15 eV. For the first time an *ab initio* polarization potential considers the polarization of the atomic core by the excited photoelectron was included in the calculation. This effect increases the photoionization cross section at the photon energy from 8 eV to 10 eV by approximately 15% and shifts the computed energies of the intermediate discrete-state resonances, bringing them to excellent agreement with the experimental energies.

DOI: 10.1103/PhysRevA.93.033408

I. INTRODUCTION

The progress in the development of free-electron laser facilities achieved during recent years [1,2] revived the interest in the description of multiphoton ionization processes. The most important parameter for the theoretical interpretation of the experimental data is the absolute value of the atomic multiphoton photoionization cross section (PICS). Several different semiempirical and model approaches have been applied to compute PICS, e.g., the scaling method based on known photoionization cross sections of He [3–6] or the local approximation for the exchange electron-electron interaction in the calculation of single-electron wave functions [7–10]. More accurate but much more complex are *ab initio* methods within the Hartree-Fock (HF) approximation with inclusion of many-electron correlations. Several particular techniques were created to perform the ab initio calculation of the multi-photon ionization cross sections with taking into account many-electron correlations. Thus, in Ref. [11] the multiphoton ionization cross section of atomic Mg were calculated applying the L^2 basis constructed from B splines. The 250 configurations of the $3sn\ell$ and $3pn\ell'$ series were considered. However, the method is restricted to the case of bivalent atoms. For the case of the two-photon ionization of Ar those calculations were performed in Refs. [12–15]. The main difficulty in the calculation of the two-photon transition amplitude to the final state with the $k\ell$ photoelectron is the summation over the complete set of intermediate states including the continuum ones. Pindzola and Kelly [12] tried to avoid this problem in the direct calculation by a proper selection of the upper limit of spatial integration and a large set of intermediate states in the numerical integration. Nevertheless, the photon-energy dependence of the two-photon PICS computed in Ref. [12] demonstrated some nonphysical curvatures (see Sec. III B below).

In Ref. [13] the two-photon ionization cross section has been calculated by the transition-matrix method where the transition amplitudes were determined applying the Dalgarno-Lewis technique [16]. Several many-electron corrections to the two-photon transition amplitude computed in the lowest order of perturbation theory (LOPT) were included. In Ref. [13] the intermediate-state integration has been made via an effective function, which was determined by the solution of an inhomogeneous integrodifferential equation. This equation is widely applicable in atomic and nuclear physics. The effective function has been differently referred to in the literature, e.g., "the perturbed-function" [17,18], "effective wave function" [13,19], "correlation function" [20]. In the present paper we call this function the "correlation function" (CF) as earlier [20]. The CF method is more precise as compared to the one of direct summation over the intermediate states [12]. However, the numerical algorithm to solve the inhomogeneous integrodifferential equation did not converge at any energy [13]. In particular, it was not possible to calculate the two-photon ionization cross section for energies close to intermediate discrete resonances acting as dominating states for the multiphoton PICS.

In the papers [21,22] the two- and three-photon ionization of H and Li were calculated. A particular approach has been applied to avoid a divergence in the Dalgarno-Lewis method in the "close-to-resonance" region. The corresponding differential equation has been solved precisely in the "between-resonance" energy regions. Then the transition amplitude was divided by nonresonant and resonant parts. The smoothly varying functions of both parts were interpolated to the regions of the intermediate resonances and the respective cross sections were obtained.

*Corresponding author: Petrov_ID@mail.ru

 ©2016 American Physical Society

A further method using variationally stable procedures with a Slater orbital basis has been applied in Ref. [14] for similar calculations. There, an important intermediate-state monopole (shake) correlation, omitted in Ref. [13], was incorporated in the calculation. That correction changed dramatically the theoretical multiphoton PICS for the transition to the $3p^5\varepsilon s(^1S)$ channel. The numerical procedure enabled us to calculate photoionization cross sections at all photon energies including intermediate resonances. However, the restriction of the Slater orbital basis set led to some inaccuracy in the calculated PICS (see Sec. III B below). Finally, in Ref. [15] the angular-distribution parameters for photoelectrons were calculated in the same approximation.

Here we introduce a method for the calculation of two-photon cross sections, which is based on the CF technique and which solves the described difficulties. It applies a noniterative numerical procedure for the solution of the inhomogeneous integrodifferential equation. The procedure is based on the reduction of the single nonlocal integrodifferential equation to a system of local differential equations as described, e.g., in [23]. The stability of this technique was recently demonstrated in the calculation of two-photon ionization of the H_2 molecule [24] in the LOPT approximation. In addition to the many-electron correlations taken into account in Refs. [14,15], the effect of atomic core polarization by the outgoing photoelectron [25] is considered.

The paper is organized as follows. In Sec. II we describe the calculation method of the two-photon ionization transition amplitudes of Ar in the LOPT applying the CF technique. In Sec. III we calculate partial and total $3p$ two-photon ionization cross sections of Ar and angular-distribution parameters for the photoelectrons. In Secs. III A and III B the details of the calculations of atomic orbitals (AOs), correlation functions, and final-state photoelectron wave functions are discussed demonstrating the advantage of the used noniterative numerical method for the CF calculation.

The calculated $3p$ two-photon ionization cross sections of Ar are presented in Sec. III C. In Sec. III D the influence of the polarization of the atomic core induced by the outgoing electron is studied in addition to the direct ionization and correlation effects. The influence of all mentioned effects on the angular-distribution parameters for the photoelectrons is studied in Sec. IV. We conclude with a brief summary in Sec. V. In the Appendix we present the equations for the CFs and the geometrical factors used in the calculation of many-electron correlations.

II. TWO-PHOTON IONIZATION TRANSITION AMPLITUDES CALCULATED BY THE CORRELATION FUNCTION METHOD

We study two-photon ionization of the $3p$ shell of Ar which can be presented by the scheme

$$\mathrm{Ar}\ 3p^6(^1S) + 2\gamma \rightarrow \mathrm{Ar}^+\ 3p^5(^2P)\varepsilon\ell(^1L) \quad (L = 0,2). \tag{1}$$

The amplitude of the two-photon ionization transition $i \rightarrow f$ with photon energy ω in the LOPT is [13,21,22]

$$T_{i\rightarrow f} = \sum_m \frac{\langle f|D|m\rangle\langle m|D|i\rangle}{E_i + \omega - E_m} \tag{2}$$

where E_i and E_m are energies of the initial and intermediate states respectively, D is the electric dipole operator, and the sum over the intermediate states m includes integration over the continuum states. The LOPT processes are

$$3p^6 \dashrightarrow 3p^5\varepsilon'\ell' \dashrightarrow 3p^5\varepsilon\ell \quad \text{(Ia)},$$

$$3s^23p^6 \dashrightarrow 3s^13p^6\varepsilon\ell \dashrightarrow 3s^23p^5\varepsilon\ell \quad \text{(Ib)},$$

where the dashed arrows denote electric dipole interaction. The solid arrow in the following equations denote Coulomb interaction. In the LS coupling scheme the general expression (2) for the process, e.g., (Ia), becomes

$$T = \sum_{\varepsilon'>F}\sum_{\ell'} \frac{\langle 3p^5\varepsilon\ell|D|3p^5\varepsilon'\ell'\rangle\langle 3p^5\varepsilon'\ell'|D|3p^6\rangle}{\omega - E_{3p}^{(i)} - \varepsilon'}, \tag{3}$$

where $E_{3p}^{(i)}$ is the ionization potential of the $3p$ electron.

In addition to the LOPT amplitudes (Ia, Ib), the complementary amplitudes of the first order over the electron-electron interaction were also included in the calculation. Those amplitudes involve all possible one- and two- electron excitations allowed by selection rules in the initial, final, and intermediate states and are listed in Ref. [14]. Two-photon transitions including many-electron correlations with the same numbering as in Ref. [14] are intermediate-state interchannel correlation:

$$3p^6 \dashrightarrow 3p^5\varepsilon''\ell'' \rightarrow 3p^5\varepsilon'\ell' \dashrightarrow 3p^5\varepsilon\ell \quad \text{(II)};$$

ground-state correlations:

$$3p^6 \rightarrow 3p^4\varepsilon'\ell'\varepsilon''\ell'' \dashrightarrow 3p^5\varepsilon'\ell' \dashrightarrow 3p^5\varepsilon\ell \quad \text{(IIIa)},$$
$$3p^6 \rightarrow 3p^4\varepsilon'\ell'\varepsilon''\ell'' \dashrightarrow 3p^4\varepsilon\ell\varepsilon''\ell'' \dashrightarrow 3p^5\varepsilon\ell \quad \text{(IIIb)},$$
$$3p^6 \rightarrow 3p^4\varepsilon\ell\varepsilon''\ell'' \dashrightarrow 3p^4\varepsilon\ell\varepsilon'\ell' \dashrightarrow 3p^5\varepsilon\ell \quad \text{(IIIc)};$$

intermediate-state shake-up correlation:

$$3p^6 \dashrightarrow 3p^5\varepsilon'\ell' \rightarrow 3p^4\varepsilon\ell\varepsilon'\ell' \dashrightarrow 3p^5\varepsilon\ell \quad \text{(IV)};$$

intermediate-state electron-scattering correlation:

$$3p^6 \dashrightarrow 3p^5\varepsilon'\ell' \rightarrow 3p^4\varepsilon\ell\varepsilon''\ell'' \dashrightarrow 3p^5\varepsilon\ell \quad \text{(V)};$$

final-state electron-scattering correlations:

$$3p^6 \dashrightarrow 3p^5\varepsilon'\ell' \dashrightarrow 3p^4\varepsilon'\ell'\varepsilon''\ell'' \rightarrow 3p^5\varepsilon\ell \quad \text{(VIa)},$$
$$3p^6 \dashrightarrow 3p^5\varepsilon''\ell'' \dashrightarrow 3p^4\varepsilon'\ell'\varepsilon''\ell'' \rightarrow 3p^5\varepsilon\ell \quad \text{(VIb)}.$$

The explicit expressions for the correlation amplitudes (II–VI) are more cumbersome than Eq. (3). For example, transition amplitude (II) is expressed as

$$T = \sum_{\varepsilon',\varepsilon''>F}\sum_{\ell',\ell''} \frac{\langle 3p^5\varepsilon\ell|D|3p^5\varepsilon'\ell'\rangle\langle 3p^5\varepsilon'\ell'|V|3p^5\varepsilon''\ell''\rangle\langle 3p^5\varepsilon''\ell''|D|3p^6\rangle}{(\omega - E_{3p}^{(i)} - \varepsilon')(\omega - E_{3p}^{(i)} - \varepsilon'')}, \tag{4}$$

where V is the perturbation operator

$$V = \sum_{i<j} r_{ij}^{-1} - u_{\rm HF}, \tag{5}$$

and $u_{\rm HF}$ in Eq. (5) is the HF potential (13). The amplitude (4) can be interpreted as an excitation of the $3p$-core electron to the virtual $\varepsilon''\ell''$ state by the first photon, the following transfer of the $\varepsilon''\ell''$ electron to the $\varepsilon'\ell'$ state by the Coulomb interaction with the core, and, finally, the transfer of the virtual $\varepsilon'\ell'$ electron to a real final state $\varepsilon\ell$ by the second photon. Other correlations shown above can be interpreted similarly.

Applying the method of [26] the expressions (3) and (4) can be simplified and presented as a product of two factors, depending on angular and radial variables respectively. The radial part of the transition amplitude can be calculated applying the CF technique which is described below.

A. LOPT process (Ia)

The transition amplitude of the process (Ia) is a product of a geometrical factor (f_q) and a radial part (t_ω):

$$T_{q,\omega}^{\rm (Ia)}(L,\ell) = \sum_{\ell'} f_q(L,\ell,\ell')\, t_\omega^{\rm (Ia)}(L,\ell,\ell'), \tag{6}$$

where $q = 0$ corresponds to the linearly polarized incident radiation and $q = \pm 1$ corresponds to circularly polarized radiation.

The geometrical factor f_q in Eq. (6) was calculated using the methods described in Ref. [26]:

$$f_q(L,\ell,\ell') = \sqrt{2(2L+1)}\begin{pmatrix} L & 1 & 1 \\ -2q & q & q \end{pmatrix}\begin{Bmatrix} \ell & L & 1 \\ 1 & \ell' & 1 \end{Bmatrix} \times (\ell\|C^{(1)}\|\ell')(\ell'\|C^{(1)}\|1) \tag{7}$$

The quantities in round brackets and curly braces in Eq. (7) are $3j$ symbols and $6j$ symbols, respectively, and $(\ell\|C^{(1)}\|\ell')$ is a submatrix element of the spherical function operator, determined in the standard phase system [26]. The numerical values of f_q for the considered cases are listed in Table I.

The radial part of the amplitude (6) is

$$t_\omega^{\rm (Ia)}(L,\ell,\ell') = \sum_{\varepsilon'>F} \frac{\langle\varepsilon\ell|d|\varepsilon'\ell'\rangle\langle\varepsilon'\ell'|d|3p\rangle}{\omega - E_{3p}^{(i)} - \varepsilon'}. \tag{8}$$

The notation $\varepsilon' > F$ denotes the summation over all unoccupied single-electron states. In Eq. (8) the term-dependent $\varepsilon\ell$ AOs were computed in the configuration $3p^5\varepsilon\ell(^1L)$. $\langle\varepsilon'\ell'|d|n\ell\rangle$ is the radial integral determined either in length ($d = r$) or velocity form ($d = \frac{d}{dr} \mp \frac{\ell_{\rm max}}{r}$, $\ell_{\rm max} = \max(\ell,\ell')$, and the signs "−" or "+" correspond to the transitions $\ell \to \ell - 1$, $\ell \to \ell + 1$) where the operator d acts on the $\varepsilon'\ell'$ function.

TABLE I. Geometrical factors $f_q(L,\ell,\ell')$ [Eq. (7)] for the case of linearly polarized incoming radiation ($q = 0$). In the case of circular polarization the factors are $f_1(2,\ell,\ell') = \sqrt{3/2}\, f_0(2,\ell,\ell')$; $f_1(0,\ell,\ell') = 0$

^1L	ℓ	ℓ'	f_0
^1S	p	s	$-\frac{\sqrt{2}}{3\sqrt{3}}$
^1S	p	d	$-\frac{2\sqrt{2}}{3\sqrt{3}}$
^1D	p	s	$\frac{2}{3\sqrt{3}}$
^1D	p	d	$\frac{2}{15\sqrt{3}}$
^1D	f	d	$\frac{2\sqrt{2}}{5}$

The radial integral $\langle\varepsilon\ell|d|\varepsilon'\ell'\rangle$ is divergent if it contains two continuum wave functions. This divergence can be avoided if the CF method is applied.

The CF is defined as

$$\phi_{\ell'}(r) = \sum_{\varepsilon'>F} \frac{P_{\varepsilon'\ell'}(r)\langle\varepsilon'\ell'|d|3p\rangle}{\omega - E_{3p}^{(i)} - \varepsilon'}. \tag{9}$$

It is calculated by solving the inhomogeneous integrodifferential equation. In the length and in the velocity form this equation is

$$(h_{\ell'} - \omega + E_{3p}^{(i)})\phi_{\ell'}(r) = -rP_{3p}(r) + \sum_{n'<F} P_{n'\ell'}(r)\langle n'\ell'|d|3p\rangle, \tag{10}$$

$$(h_{\ell'} - \omega + E_{3p}^{(i)})\phi_{\ell'}(r) = \frac{dP_{3p}(r)}{dr} \pm \frac{\ell_{\rm max}}{r}P_{3p}(r) + \sum_{n'<F} P_{n'\ell'}(r)\langle n'\ell'|d|3p\rangle, \tag{11}$$

respectively, where $h_{\ell'}$ is the Hartree-Fock operator for the $\varepsilon'\ell'$ function in the configuration $3p^5\varepsilon'\ell'(^1P)$. The notation $n' < F$ means the summation over all occupied states of the atomic core.

We introduce the HF operator as in Ref. [27] Eqs. (5.32) and (5.33):

$$h_{\rm HF} = -\frac{\nabla^2}{2} - \frac{Z}{r} + u_{\rm HF}, \tag{12}$$

where the HF potential is determined via its matrix element

$$\langle i|u_{\rm HF}|j\rangle = \sum_{b<F}\left(\langle ib|r_{12}^{-1}|jb\rangle - \langle bi|r_{12}^{-1}|jb\rangle\right). \tag{13}$$

After the integration over the angular variables the radial part of the HF operator acting on the radial orbital $P_\ell(r)$ is determined as

$$h_\ell P_\ell(r) = \left(-\frac{1}{2}\frac{d^2}{dr^2} - \frac{Z}{r} + \frac{1}{2}\frac{\ell(\ell+1)}{r^2} + V_\ell(r) - X_\ell(r)\right)P_\ell(r). \tag{14}$$

Here $V_\ell(r)$ is the local part of the Coulomb interaction with the core electrons; $X_\ell(r)$ is the nonlocal part of the Coulomb interaction.

The signs in Eq. (11) correspond to the above comments to Eq. (8): in this case the sign "+" is taken if $\ell' = 0$ and "−" is taken if $\ell' = 2$. After computing the correlation function the expression for the radial part of the transition amplitude (6) becomes

$$t_\omega^{\rm (Ia)}(L,\ell,\ell') = \langle\varepsilon\ell|d|\phi_{\ell'}\rangle. \tag{15}$$

B. LOPT process (Ib)

Similar to Eq. (6), the transition amplitude of the process (Ib) is a product of two terms:

$$T^{(\mathrm{Ib})}_{q,\omega}(L) = -f_q(L,1,0)\, t^{(\mathrm{Ib})}_{\omega}(L), \tag{16}$$

where the $f_q(L,1,0)$ are listed in Table I.

The radial part of the transition amplitude (16) is

$$t^{(\mathrm{Ib})}_{\omega}(L) = \frac{\langle \varepsilon p|d|3s\rangle\langle 3s|d|3p\rangle}{\omega - E^{(i)}_{3s} - \varepsilon}, \tag{17}$$

where $E^{(i)}_{3s}$ is the ionization potential of the $3s$ electron.

It is well known [28,29] that $3s$ single-electron ionization of Ar is strongly influenced by $3p3p$-$3s\varepsilon d/s$ excitations. This many-electron effect shifts the main peak in the $3s$ photoelectron spectrum and provides an extended satellite structure. However, the mean energy of the structure is approximately equal to the HF $3s$-ionization energy. Therefore, we set the ionization potential $E^{(i)}_{3s}$ to its HF value which equals 2.555 Ry. This substitution of the HF value of $E^{(i)}_{3s}(\mathrm{HF}) = 2.555$ Ry on the experimental one $E^{(i)}_{3s}(\mathrm{expt.}) = 2.149$ Ry [30] leads to a very small change in the calculated generalized cross sections. Thus, for the $3p^5\varepsilon p(^1S)$ channel it does not exceed 0.01%.

C. Correlation processes of the third order of perturbation theory

The equations for the transition amplitudes of all the correlation processes (II)–(VI) have also a factorized form:

$$T^{(\mathrm{corr})}_{q,\omega}(L,\ell) = \sum_{l'} f_q(L,\ell,\ell') \sum_{\ell''} t^{(\mathrm{corr})}_{\omega}(L,\ell,\ell',\ell''). \tag{18}$$

The geometrical factor f_q is identical for all correlation processes (II)–(VI) and is listed in Table I. The radial parts $t^{(\mathrm{corr})}_{\omega}(L,\ell,\ell',\ell'')$ depend on both ℓ' and ℓ'' intermediate quantum numbers. The calculation of $t^{(\mathrm{corr})}_{\omega}$ is individual for each correlation process (II)–(VI) and is described in detail in the Appendix.

III. TWO-PHOTON IONIZATION CROSS SECTIONS OF 3p SHELL OF ARGON

The cross section describing two-photon ionization has the dimension cm^2 [12] and contains the photon flux. In order to compare our calculation with results of work [13,14] we use, as in these papers, the generalized two-photon ionization cross section (G2PICS) which has the dimension cm^4 s and does not contain the photon flux. The G2PICS is a sum of partial cross sections:

$$\sigma_q(\omega) = \sum_{L,\ell} \sigma_q(L,\ell,\omega). \tag{19}$$

where each of partial G2PICS is determined by

$$\sigma_q(L,\ell,\omega) = \frac{8\pi^3\alpha a_0^5}{c}\omega^{\pm 2}|T_{q,\omega}(L,\ell)|^2. \tag{20}$$

In Eq. (20) $\alpha = 1/137.036$ is a fine-structure constant; $a_0 = 5.291\,77 \times 10^{-9}$ cm is the Bohr radius; $c = 2.997\,92 \times 10^{10}$ cm/s is light velocity in vacuum; ω is exciting photon energy in atomic units; + and − correspond to the length and velocity form of the electrical dipole operator, respectively. The two-photon transition amplitude $T_{q,\omega}(L,\ell)$ is then

$$T_{q,\omega}(L,\ell) = T^{(\mathrm{Ia})}_{q,\omega}(L,\ell) + T^{(\mathrm{Ib})}_{q,\omega}(L,\ell) + \sum_{(\mathrm{corr})} T^{(\mathrm{corr})}_{q,\omega}(L,\ell), \tag{21}$$

where terms on the right-hand side are calculated via Eqs. (6), (16), and (18), and the index "corr" denotes the correlation amplitudes (II)–(VI). The radial parts t_ω of the transition amplitudes (6), (16), and (18) contain electric dipole integrals and energy denominators in atomic units.

A. Calculational details

Core AOs were obtained by solving the nonrelativistic HF equation for the configuration $1s^22s^22p^63s^23p^6$ and remained frozen in the calculation. Continuum electron wave function were calculated by solution of the term-dependent HF equation for the configurations $3p^5\varepsilon p(^1S)$, $3p^5\varepsilon p(^1D)$, and $3p^5\varepsilon f(^1D)$. These AOs have the following asymptotic form:

$$P_{\varepsilon\ell}(r) \xrightarrow{r\to\infty} \sqrt{\frac{2}{\pi k}} \sin\left(kr - \frac{\ell\pi}{2} + \frac{Z_{as}}{k}\ln(2kr) + \delta_\ell\right). \tag{22}$$

Here k is a wave vector of the continuum electron in a.u.; Z_{as} is the asymptotic charge of the ion; δ_ℓ represents the sum

$$\delta_\ell = \arg\Gamma\left(\ell + 1 - \imath\frac{Z_{as}}{k}\right) + \varphi_\ell, \tag{23}$$

where φ_ℓ is the short-range phase shift.

The intermediate states were taken into account using the CF method with the HF operator for the configurations $3p^5\varepsilon' s(^1P)$ and $3p^5\varepsilon' d(^1P)$. The HF operator $h_{\ell'}$ for the $\varepsilon'\ell'$ function and corresponding CF [see, e.g., Eqs. (10) and (11)] includes local J_k and nonlocal (exchange) K_k parts of the Coulomb interaction operator with core electron (i):

$$\begin{aligned} J_k(P_i;r)\phi_{\ell'}(r) &= y_k(P_i,P_i;r)\,\phi_{\ell'}(r) \\ &= \int_0^\infty \frac{r_<^k}{r_>^{k+1}} P_i(r')\,P_i(r')\,dr'\,\phi_{\ell'}(r), \end{aligned} \tag{24}$$

$$\begin{aligned} K_k(P_i;r)\phi_{\ell'}(r) &= y_k(P_i,\phi_{\ell'};r)P_i(r) \\ &= \int_0^\infty \frac{r_<^k}{r_>^{k+1}} P_i(r')\phi_{\ell'}(r')\,dr'\,P_i(r), \end{aligned} \tag{25}$$

where $r_<$ and $r_>$ is the lesser and the greater of the r and r'.

To solve Eqs. (10) and (11) with the nonlocal part of electron-electron interaction we applied a technique described in Ref. [23]. We introduced the function

$$Y_k(P_i,\phi_{\ell'};r) = r\,y_k(P_i,\phi_{\ell'};r), \tag{26}$$

which satisfies the following differential equation:

$$\begin{aligned} \frac{d^2Y_k(P_i,\phi_{\ell'};r)}{dr^2} &= k(k+1)Y_k(P_i,\phi_{\ell'};r) \\ &\quad - \frac{2k+1}{r}P_i(r)\,\phi_{\ell'}(r) \end{aligned} \tag{27}$$

with boundary conditions

$$Y_k(P_i,\phi_{\ell'};r) = A_k\,r^{k+1} \quad (r\to 0), \tag{28}$$

$$Y_k(P_i,\phi_{\ell'};r) = A_k\,r^{-k} \quad (r\to\infty). \tag{29}$$

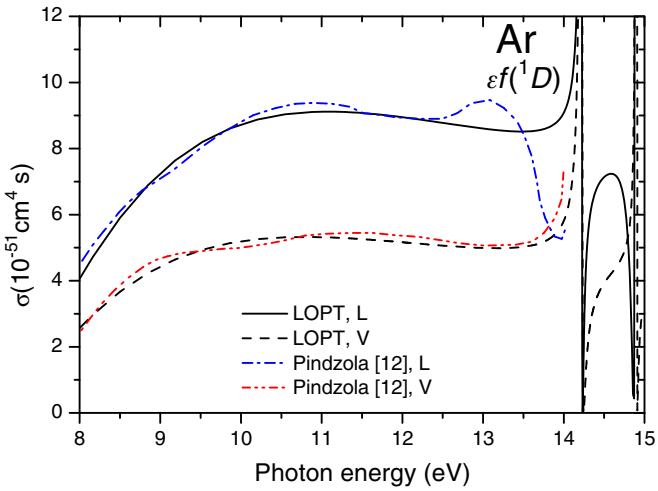

FIG. 1. The $3p$ G2PICS for the transition to the $\varepsilon f(^1D)$ channel calculated in the LOPT approximation in present work and in the paper [12] in the length (L) and velocity (V) forms of the dipole transition operator and for the linearly polarized incoming radiation.

Thereby, the nonlocal integrodifferential equations (10) and (11) are transformed to a system of local differential equations. The numerical solution of the system is noniterative, stable, and converges at each energy including the resonance regions.

B. Advantage of the noniterative method of the CF calculation

In this section we present the results of our calculation of the $3p$ G2PICS of Ar, performed within the LOPT [processes (Ia) and (Ib) are considered only] and they will be compared with preceding calculations in order to check the quality and stability of the algorithms.

In Ref. [12] the transition amplitudes (2) were calculated using direct numerical integration. To obtain the required accuracy Pindzola and Kelly [12] selected a particular cutoff radius $R_{\max}$ and a number of mesh points in the numerical radial integration.

In Fig. 1 the partial G2PICS for the $\varepsilon f(^1D)$ final-state channel calculated in Ref. [12] and in the present work are compared. Only LOPT process and linearly polarized incoming radiation were considered. A good overall agreement between results of both calculations exists. However, the data of [12] display nonphysical beats, whereas our data are smoother in the out-of-resonance region.

In Fig. 2(a) partial G2PICS for the $\varepsilon p(^1S)$ channel calculated in Ref. [13] (dash-dotted curve) are compared with our calculation (solid line). The length form of the electric dipole operator and the CF method were applied in both calculations, and the process (Ia) was taken into account only. The G2PICS computed by us and by Starace and Jiang [13] are in very good agreement if we set the computed energy of the $3p^54s(^1P)$ resonance to its experimental value 11.62 eV (see Table III from [13]). For this purpose we changed the HF value of the $3p$ ionization potential, $E_{3p}^{(i)} = 1.182$ Ry, by the $\Delta E_{3p}^{(i)} = -0.045$ Ry (note that the HF value is $\varepsilon_{4s} = -0.283$ Ry). With this value of $E_{3p}^{(i)}$ the denominator in Eq. (8) becomes equal to zero at $\omega = 11.62$ eV. The HF and experimental energy positions of the intermediate $3p^54s(^1P)$ resonance are marked in Fig. 2(a) as vertical lines.

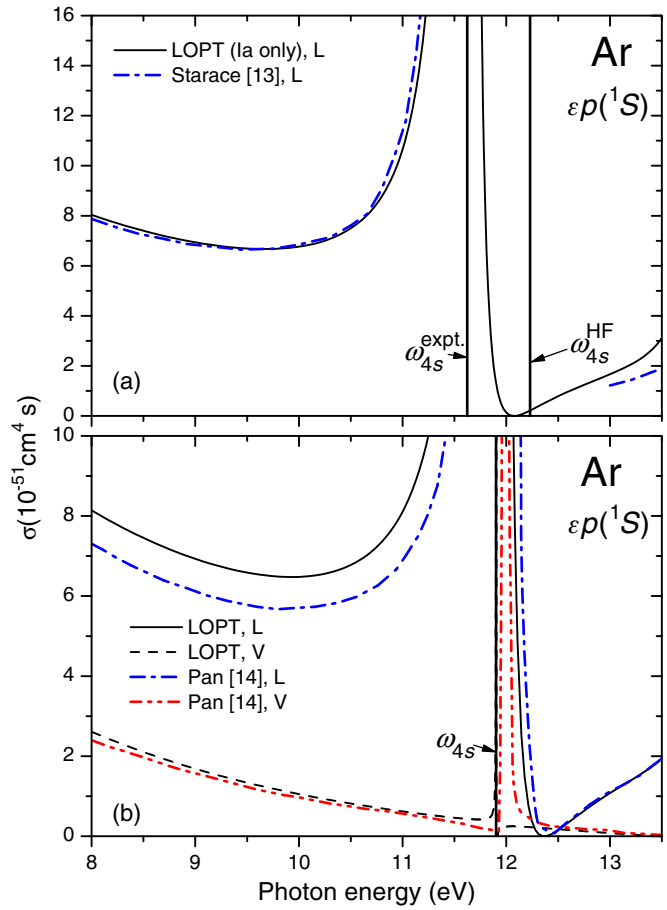

FIG. 2. The $3p$ partial G2PICS for the transition to the $\varepsilon p(^1S)$ channel and for the linearly polarized incoming radiation calculated in the LOPT. (a) Length form (L) of the dipole transition operator: our calculation performed using the experimental position of the $3p^54s(^1P)$ resonance, and data from [13]. The HF and experimental values of intermediate discrete $3p^54s(^1P)$ resonance are marked by vertical lines. (b) Length (L) and velocity (V) forms of the dipole transition operator: our calculation (LOPT) and data from [14]. The experimental ionization potential $E_{3p}^{(i)} = 1.158$ Ry was used in the calculation. The respective position of the intermediate discrete $3p^54s(^1P)$ resonance is marked by a vertical line.

In Ref. [13] it was noticed that the applied Dalgarno-Lewis algorithm [16] for the CF calculation was found to be divergent at the region of intermediate discrete resonances. Therefore, in Fig. 2(a) the G2PICS dependency shows breaks. The same situation appeared in our work when the nonlocal exchange potential (25) was included via an iteration procedure. Within the noniterative numerical scheme of CF calculation (see Sec. III A) we successfully computed the CF and G2PICS at any energy including the regions of the resonances until $E_R \pm 2.5$ meV, where E_R is the exact energy of the resonance.

The generalized two-photon ionization cross section for the transition to the $\varepsilon p(^1S)$ channel calculated in the HF approximation by us and in paper [14] are presented in Fig. 2(b) in the length and velocity form of the dipole transition operator. In both calculations the HF value of $E_{3p}^{(i)}$ was used. In our calculation we used the noniterative CF method. In the paper [14] the variationally stable procedures on a basis of Slater orbitals was applied which also made it possible to avoid

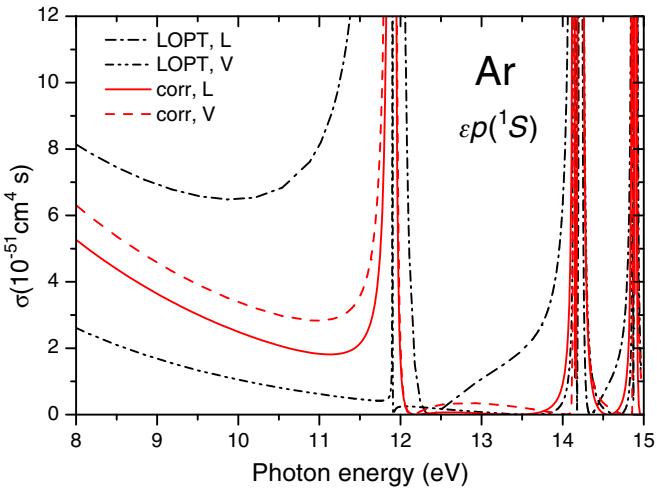

FIG. 3. The $3p$ partial G2PICS for the transition to the $\varepsilon p(^1S)$ channel and for linearly polarized incoming radiation calculated in LOPT and with taking into account many-electron correlations (corr). Both length (L) and velocity (V) forms are presented.

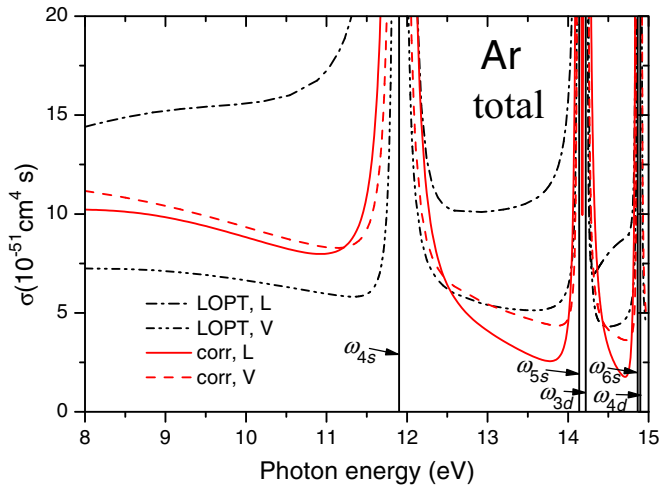

FIG. 4. The $3p$ total G2PICS in length (L) and velocity (V) form for the linearly polarized incoming radiation calculated in LOPT and with taking into account many-electron correlations (corr). Vertical lines: the energies of the intermediate $3p^5n\ell(^1P)$ resonances calculated using the experimental value of $3p$ ionization potential $E^{(i)}_{3p} = 1.158$ Ry.

the divergence of the calculation in the "close-to-resonance" region.

Comparing our G2PICSs with [14] we draw attention to the following:

(i) The G2PICS calculated in Ref. [14] in length form are approximately 12% smaller than our G2PICS in the 8–11.5 eV photon energy range.

(ii) Our G2PICS (dashed line) displays in velocity form a very sharp peak at the ω_{4s} with the width not exceeding 0.01 eV [in Fig. 2(b) this resonance is blended by the vertical line ω_{4s}]. It is much broader in the calculation of [14].

(iii) The results of [14] reproduce the energy position of the $3p^54s(^1P)$ intermediate resonance $\omega_{4s} = 11.90$ eV worse than our calculation which is even more evident for the velocity form of the calculated G2PICS: the shift comprises approximately 0.08 eV [see dash-double-dotted curve in Fig. 2(b)].

These discrepancies are most likely due to a limited set of Slater functions applied in Ref. [14] in the variationally stable procedure.

C. Influence of many-electron correlations

Now we discuss all transitions (I)–(VI) that were taken into account in calculating the G2PICS. We note that we chose the experimental potential of double ionization of the Ar $3p^4(^3P_2)$ level $E^{(i)}_{3p^2} = 3.189$ Ry [30] not only in the calculation of the (VIa) and (VIb) amplitudes but also for the (III)–(V) processes whereas in Ref. [14] the approximation $E^{(i)}_{3p^2} = 2E^{(i)}_{3p}$ was applied for the latter cases.

The strongest influence of many-electron correlations is seen in the G2PICS of the $\varepsilon p(^1S)$ channel (Fig. 3). The LOPT G2PICS in length form (dash-dotted curve) at the threshold is almost four times larger than in the velocity form (dash-double-dotted curve). After inclusion of many-electron effects [processes (II)–(VI)] this difference is reduced down to 20% (solid and dashed curves respectively). The influence of many-electron effects on the computed values of G2PICSs for the $\varepsilon p(^1D)$ and $\varepsilon f(^1D)$ is less pronounced (see Sec. III D).

The influence of many-electron correlations on the total G2PICSs of the $3p$ shell of Ar for the linear polarization of exciting radiation is presented in Fig. 4. The changes are similar to the case of $\varepsilon p(^1S)$ channel. If one takes into account the LOPT processes only [(Ia) and (Ib)] the total G2PICS computed in the length form (dash-dotted curve) exceeds at the threshold almost twice that in the velocity form (dash-double-dotted curve). After accounting for many-electron effects [processes (II)–(VI)] the difference is decreased to 8% at the 8–11-eV photon energy region (solid and dashed curves respectively).

In Fig. 5 the presently calculated total cross sections and those of [14] with inclusion of many-electron effects are presented for the case of linearly polarized incident radiation. The results are quite close to each other. However, again a small energy difference of the intermediate $3p^54s(^1P)$ resonance obtained in [14] with respect to ours might be caused by the limited number of Slater functions in Ref. [14].

D. Atomic core polarization due to the photoelectron

Atomic core polarization was considered by implementation of an *ab initio* core polarization potential $V^{CP}(r)$ [25] in the HF operator $h_{l'}$ or $h_{l''}$ entering Eqs. (10), (11), (A5), (A8), (A9), (A10), and (A13). In addition, the matrix elements of Coulomb interaction, describing the correlations (II)–(VI), have been reduced by a factor of 1.25. By this scaling we took into account the correlation effects of higher orders as it was described in Refs. [20,25,31].

The scaling factor was obtained by taking into account the correlation corrections to the matrix element $V(Im_I, Km_K)$ of the Coulomb interaction between the configurations I and K [m_I and m_K are total and inner (intermediate) angular momenta of electrons of the I and K configurations]. The

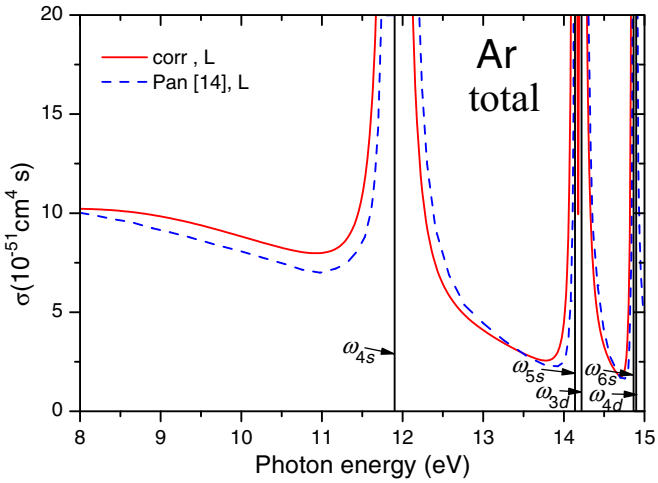

FIG. 5. The $3p$ total G2PICS in the length (L) form for linearly polarized incoming radiation calculated with taking into account many-electron correlations. The results of our calculation (corr) and those of [14] are compared. Vertical lines: the energies of the intermediate $3p^5n\ell(^1P)$ resonances calculated using the experimental value of $3p$ ionization potential $E_{3p}^{(i)} = 1.158$ Ry.

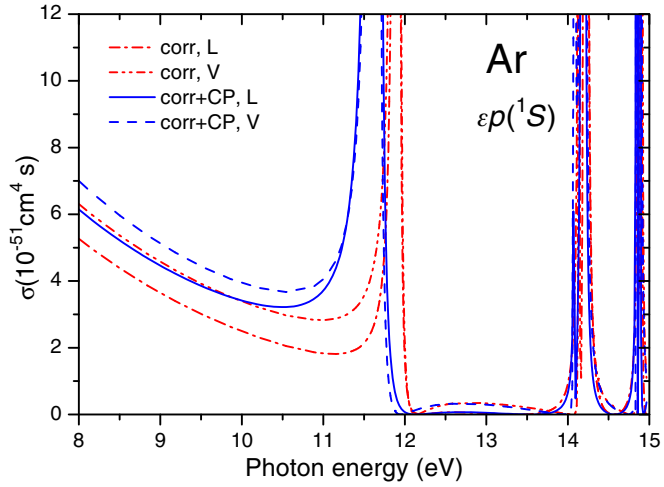

FIG. 6. The $3p$ partial G2PICS for the $\varepsilon p(^1S)$ channel in length (L) and velocity (V) form for linearly polarized incoming radiation calculated with taking into account many-electron correlations (corr) and, in addition, polarization of the atomic core by the photoelectron (corr + CP).

correction ΔV to the matrix element $V(Im_I,Km_K)$ was calculated applying the second-order perturbation theory formula similar to Eq. (2):

$$\Delta V(Im_I,Km_K) = \sum_{Xm_X} \frac{\langle Im_I|V|Xm_X\rangle\langle Xm_X|V|Km_K\rangle}{E(I)-E(X)}, \tag{30}$$

where the summation runs over the discrete and continuum states of the configuration X, and $E(I)$ and $E(X)$ are mean HF energies of the I and X configurations, respectively. The correction ΔV, usually, has the opposite sign with respect to the matrix element V. Therefore, taking into account this correction can be treated as the effective decrease of the interaction between the I and K states. The scaling factor for this interaction was computed using the "Dyson-type" equation, supposing that scaling is the same for all interactions entering Eq. (30):

$$\frac{V(Im_I,Km_K)}{k} = V(Im_I,Km_K) + \frac{\Delta V(Im_I,Km_K)}{k}. \tag{31}$$

The latter approximation appeared to be a very reasonable [20,25,31].

In Fig. 6 the core polarization increases the calculated partial G2PICS for the $\varepsilon p(^1S)$ channel by 17% for the length form (dash-dotted and solid curves) and by 11% for the velocity form (dash-double-dotted and dashed curves). It also shifts the calculated energy position of the intermediate resonances to lower photon energies. The reason is that the photoelectron distorts the core electrons. Therefore, the core-electron potential is changed and it leads to a stronger localization of the photoelectron AO.

In Fig. 7 the influences of correlation and polarization effects are demonstrated for the $\varepsilon p(^1D)$ channel in the length form. Many-electron correlations [processes (II)–(VI)] shifted the computed first minimum in the G2PICS by 0.7 eV to the threshold and decreased at the threshold by 28% (cf. dashed and dash-dotted curves). The polarization of the atomic core induces an additional shift of the theoretical minimum by 0.2 eV (cf. dash-dotted and solid curves), but the threshold G2PICSs remained almost unchanged. Similar to the case of the $\varepsilon p(^1S)$ channel the core polarization shifted the calculated energy position of the intermediate resonances by the same value towards lower photon energies.

In Fig. 8 the same effect is presented for the $\varepsilon f(^1D)$ channel. The many-electron correlations decrease the computed G2PICSs by 17% at the threshold and by 36% at the $\omega = 11$ eV (dashed and dash-dotted curves). Besides, the prominent resonance profile that corresponds to the intermediate $3p^54s(^1P)$ state becomes apparent. The origin of that profile is connected to the intermediate-state interchannel correlation (II). The same result was obtained in Ref. [14]. The core polarization

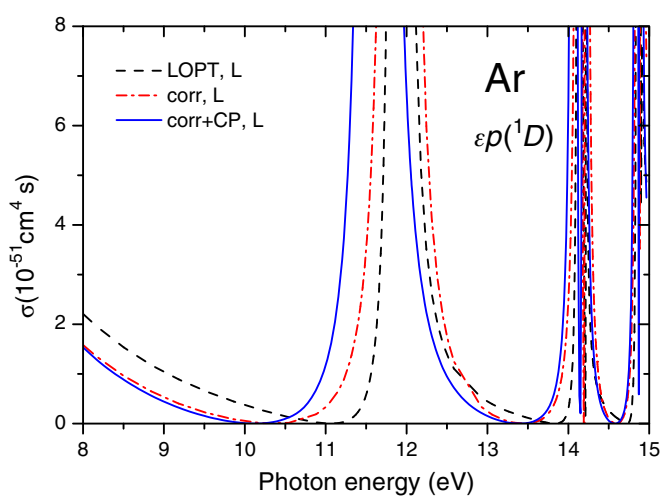

FIG. 7. The $3p$ partial G2PICS for the $\varepsilon p(^1D)$ channel in length (L) form for linearly polarized incoming radiation calculated in LOPT, with taking into account many-electron correlations (corr) and, in addition, polarization of the atomic core by the photoelectron (corr + CP).

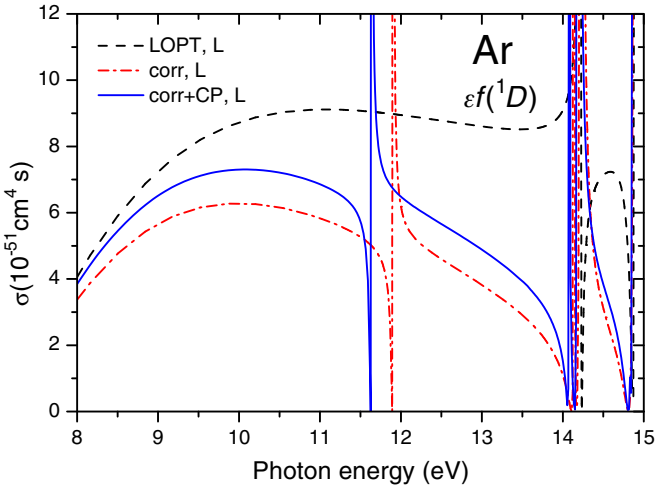

FIG. 8. The $3p$ partial G2PICS for the $\varepsilon f(^1D)$ channel in length (L) form for linearly polarized incoming radiation calculated in LOPT, with taking into account many-electron correlations (corr) and, in addition, polarization of the atomic core by the photoelectron (corr + CP).

provided an increase of the theoretical G2PICSs by 16% in the 8–11 eV photon energy range (cf. dash-dotted and solid curves) and a shift of the intermediate discrete state resonances, as in the case of the $\varepsilon p(^1S)$ and $\varepsilon p(^1D)$ channels.

In Fig. 9 the core polarization effect is demonstrated for the total $3p$ G2PICSs of Ar which are increased in length (cf. dash-dotted and solid curves) and velocity (cf. dash-double-dotted and dashed curves) forms by 18% and 15% respectively at $\omega = 9.5$ eV. The main effect of the core polarization is a shift of computed energy positions of the intermediate discrete resonances to the low-energy side. In Fig. 9 the vertical lines mark the experimental energies of the $3p^5_{3/2}nl'[3/2]_1$ resonances [30]. In Fig. 10 the total G2PICSs are presented in logarithmic scale. One can see an excellent agreement between

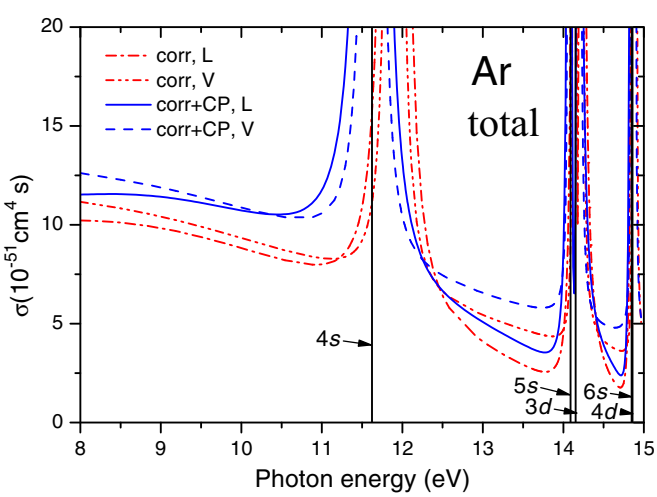

FIG. 9. The $3p$ total G2PICS in the length (L) and velocity (V) form for linearly polarized incoming radiation calculated with taking into account many-electron correlations (corr) and, in addition, polarization of the atomic core by the photoelectron (corr + CP). Vertical lines: experimental energy positions of the intermediate resonances [30].

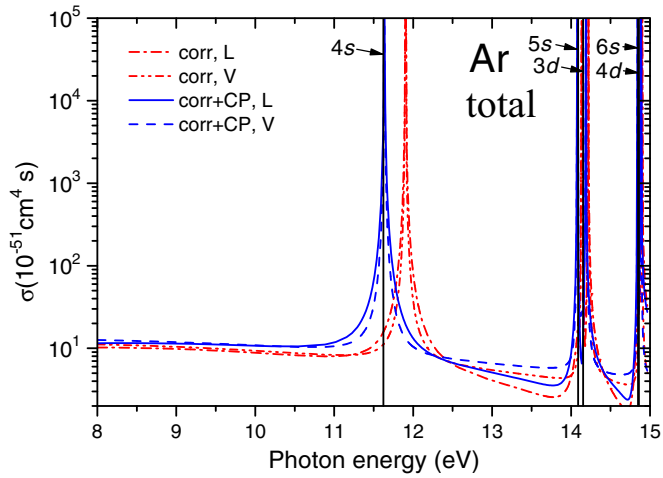

FIG. 10. The same as in Fig. 9 but in logarithmic scale for G2PICS.

the measured and calculated energy positions of resonances after accounting for core polarization.

In our calculation of the ionization transition amplitudes the radiation widths of the intermediate resonances were not taken into account because of their dependence on the incoming laser radiation intensity [32]. Applying equations from the paper [32] we have estimated the accuracy of our approximation in the energy region of the $3p^54s(^1P)$ resonance. If the duration of the laser impulse is more than 1.5 fs and the intensity is less than 10^{12} W/cm^2 our approximation in the G2PICS calculation is accurate within less than 5% outside the photon-energy range $\omega_{4s} \pm 0.25$ eV which remains Fig. 9 unchanged.

IV. ANGULAR-DISTRIBUTION OF PHOTOELECTRONS

The expression for the differential G2PICS is

$$\frac{d\sigma_q(\omega)}{d\Omega} = \frac{\sigma_q(\omega)}{4\pi}\left[1 + \beta_2^q(\omega)P_2(\cos\theta) + \beta_4^q(\omega)P_4(\cos\theta)\right], \quad (32)$$

where β_λ^q are the angular distribution parameters for photoelectrons, P_λ is the Legendre polynomial, θ is the angle between the momentum of photoelectron and electric-field vectors for the linearly polarized incident radiation ($q = 0$) or between the momentum of photoelectron and the direction of propagation vectors of the circularly polarized incoming radiation ($q = \pm 1$).

The expression for the photoelectron angular distribution parameters was obtained using a method similar to that described in Ref. [15]:

$$\beta_\lambda^q(\omega) = \frac{8\pi^3\alpha a_0^5}{c\sigma_q(\omega)}\omega^{\pm 2}\sum_{\ell\ell' LL'}(-1)^{L-2q+L'+L_c} \times[\lambda]([\ell][\ell'][L][L'])^{1/2}e^{i(\delta_\ell-\delta_{\ell'})} \times\begin{pmatrix}\lambda & \ell & \ell'\\ 0 & 0 & 0\end{pmatrix}\begin{pmatrix}\lambda & L & L'\\ 0 & -2q & 2q\end{pmatrix}\begin{Bmatrix}\lambda & L & L'\\ L_c & \ell' & \ell\end{Bmatrix} \times T_{q,\omega}(L,\ell)\,T^*_{q,\omega}(L',\ell'). \quad (33)$$

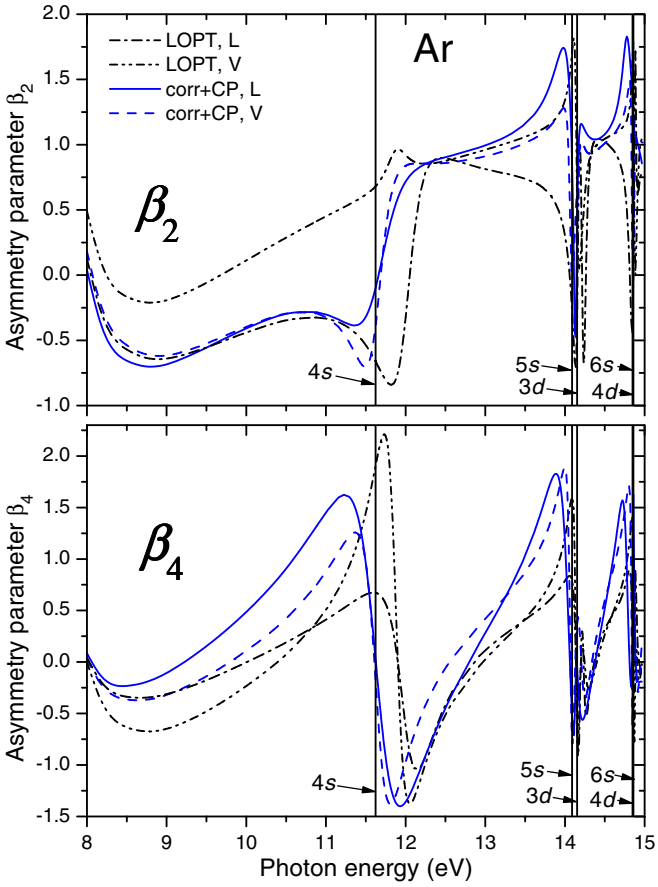

FIG. 11. Angular distribution parameters for photoelectrons for the $3p$-two-photon ionization of Ar in the length (L) and velocity (V) form for the linearly polarized incoming radiation calculated in the LOPT and with taking into account many-electron correlations and core polarization (corr + CP). Vertical lines: experimental energy positions of the intermediate resonances [30].

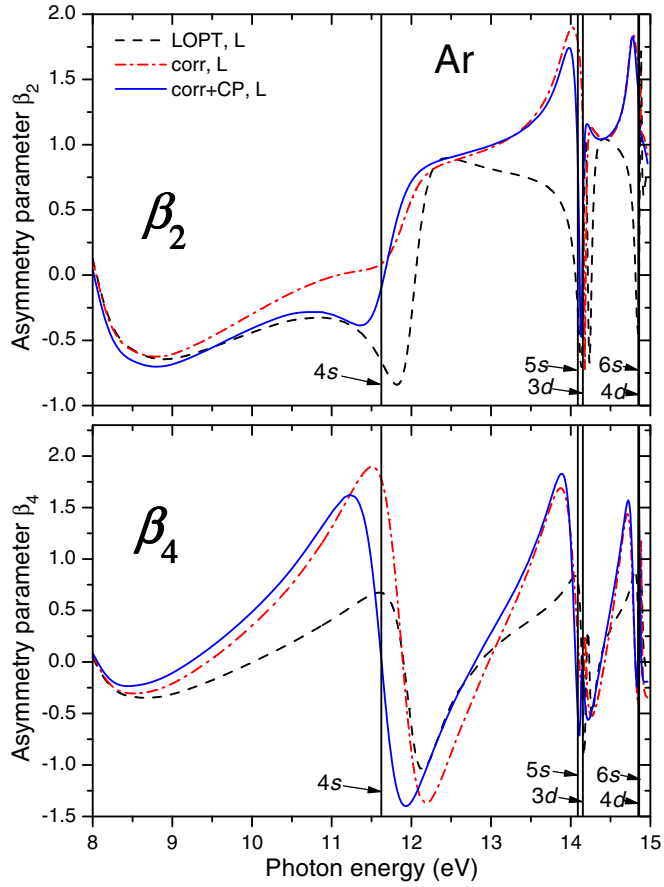

FIG. 12. Angular distribution parameters for photoelectrons for the $3p$-two-photon ionization of Ar in the length (L) form for the linearly polarized incoming radiation calculated in the LOPT, with taking into account many-electron correlations (corr) and, in addition, polarization of atomic core by the outgoing photoelectron (corr + CP).

In Eq. (33) $[x] \equiv 2x + 1$, L_c is the orbital momentum of the Ar $3p^5$ ionic core (in this case $L_c = 1$). The only difference between Eq. (33) and Eq. (10) in Ref. [15] is that in our work the standard phase system for the spherical harmonics [26] was applied (the rank of the operator is enclosed in brackets). The interrelation with the spherical harmonic in the pseudostandard phase system applied in Ref. [15] is

$$Y_m^{(\ell)} = i^\ell Y_{\ell m}. \tag{34}$$

In addition, in Eq. (33) it was considered that after absorption of two photons having polarization q the projection of the final-state $3p^5\varepsilon\ell(^1L)$ total momentum M equals $2q$.

The β_2 and β_4 parameters calculated in the LOPT [processes (Ia) and (Ib) are only considered] for the case of linear polarization of incoming radiation are plotted in Fig. 11 (dash-dotted curve and dash-double-dotted curve for the length and velocity form, respectively). The total influence of many-electron correlations [processes (II)–(VI)] and core polarization on the β parameters is also depicted in the same figure (solid and dashed lines for the length and velocity form, respectively).

Taking into account many-electron effects and core polarization results in much better agreement between β parameters computed in the length and velocity forms. It is especially apparent for the β_2 parameter.

An individual influence of many-electron effects and core polarization on the calculated β parameters is presented in Fig. 12 for the case of linearly polarized incoming radiation in the length form. The many-electron correlations (II)–(VI) change considerably the parameters computed in the LOPT (dash-dotted and dashed line, respectively). The core polarization provides an opposite effect, returning the β_2 parameter back to the LOPT values. However, as in the case of G2PICS, the main influence of the core polarization is the shift of the $\beta(\omega)$ dependencies towards the threshold, which is particularly noticeable for the β_4 parameter.

One should note that we also studied the manifestation of many-electron correlations and core polarization for circularly polarized incoming radiation ($q = \pm 1$). We do not present those results, to avoid the excessive bulkiness of the paper, and restrict to a short comment. The mentioned manifestation was found to be less pronounced due to forbidden transition to the $\varepsilon p(^1S)$ channel. The changes of the computed G2PICS and β parameters are similar to those for linearly polarized incoming radiation but they are somewhat weaker. The energy shifts of the intermediate discrete resonances due to the core

TABLE II. The values of the a_1 and b_2 coefficients entering Eq. (A1).

ℓ	ℓ'	ℓ''	a_1	b_2
p	s	d	$\frac{4}{3}$	$-\frac{2}{5}$
p	d	s	$\frac{2}{3}$	$-\frac{1}{5}$
f	d	s	$\frac{2}{3}$	$-\frac{1}{5}$

TABLE III. The c_k coefficients entering Eq. (A7).

ℓ	ℓ'	ℓ''	c_1	c_3
p	s	s	$\frac{1}{3}$	0
p	s	d	$\frac{2}{3}$	0
p,f	d	s	$\frac{1}{3}$	0
p,f	d	d	$\frac{19}{15}$	$-\frac{9}{35}$

polarization are of cause the same for both linear and circular polarizations.

V. CONCLUSIONS

In the present paper we created a method and computer code for the calculation of the cross sections and angular distribution of photoelectrons for the two-photon ionization processes. The method is based on the application of the noniterative correlation-function technique to computing both the two-photon transition amplitudes and the many-electron correlations. The generalized cross sections, G2PICS, and the photoelectron angular distribution parameters for the two-photon ionization of the $3p$ shell of Ar were calculated. The exciting-photon energy range is limited from 8 to 15 eV and covers several intermediate discrete resonances. This method has no restrictions noted in the preceding papers [12–14] and provides reliable two-photon photoionization cross sections at all photon energies in this region including the close-to-resonance parts. The created method allowed us to take into account the atomic core polarization in the two-photon ionization of the $3p$ shell of Ar by including an *ab initio* polarization potential to the CF equations [25]. Taking core polarization into account resulted in an increase of the computed two-photon photoionization total cross section by approximately 17% at the threshold, and in a very good agreement between computed and measured energies of the intermediate resonances. The method can be easily adopted for taking into account the main relativistic effects in Pauli-Fock approximation and is planned to be applied for the calculation of the two-photon ionization cross sections of heavy atoms which are already measured and available in the literature.

ACKNOWLEDGMENTS

The work was supported by the Hessen State Initiative for the Development of Scientific and Economic Excellence (LOEWE) in the LOEWE-Focus ELCH. I.D.P., B.M.L., and V.L.S. would like to thank the Institute of Physics, University of Kassel for the hospitality. V.L.S. appreciates support from Southern Federal University within Inner Project No. 213.01.-07.2014/11PPIG. I.D.P. and B.M.L. appreciate support from Grant No. 16-02-00666-a of the RFBR. We are grateful to Prof. A. Starace for providing figures from [13–15] as highly resolved graphs. We are thankful to Prof. Ph. V. Demekhin for verification of our calculation for the εp AO in the configuration $3p^5\varepsilon p(^1S)$.

APPENDIX

In this Appendix the expressions for the radial parts of correlation transition amplitudes (II)–(VI) are presented. The methods of their calculations are also discussed.

1. Intermediate-state interchannel correlation process (II)

The radial part of the transition amplitude is

$$t_\omega^{(\mathrm{II})}(L,\ell,\ell',\ell'') = \sum_{\varepsilon',\varepsilon''>F} \frac{\langle\varepsilon\ell|d|\varepsilon'\ell'\rangle[a_1\langle\varepsilon'\ell'|y_1(3p,\varepsilon''\ell'')|3p\rangle + b_2\langle\varepsilon'\ell'|y_2(3p,3p)|\varepsilon''\ell''\rangle]\langle\varepsilon''\ell''|d|3p\rangle}{(\omega - E_{3p}^{(i)} - \varepsilon')(\omega - E_{3p}^{(i)} - \varepsilon'')}. \tag{A1}$$

In Eq. (A1) y_k operators are determined in accord with Eqs. (24) and (25). The matrix element including the y_k function is expressed by Slater integrals:

$$\langle n_3\ell_3|y_k(n_1\ell_1,n_2\ell_2)|n_4\ell_4\rangle = R^k(n_1\ell_1,n_3\ell_3;n_2\ell_2,n_4\ell_4) = \int_0^\infty dr\, P_{n_3\ell_3}(r)P_{n_4\ell_4}(r)y_k(n_1\ell_1,n_2\ell_2,r). \tag{A2}$$

Coefficients a_1 and b_2 entering equation (A1) were determined using the effective operators method [27,33]. The quantities of the coefficients are listed in Table II.

Amplitude (A1) was calculated using two CFs. The first CF $\phi_{\ell''}$ is the solution of Eqs. (10) and (11) rewritten for $\phi_{\ell''}$. With this CF equation (A1) takes the form

$$t_\omega^{(\mathrm{II})}(L,\ell,\ell',\ell'') = \sum_{\varepsilon'>F} \frac{\langle\varepsilon\ell|d|\varepsilon'\ell'\rangle[a_1\langle\varepsilon'\ell'|y_1(3p,\phi_{\ell''})|3p\rangle + b_2\langle\varepsilon'\ell'|y_2(3p,3p)|\phi_{\ell''}\rangle]}{(\omega - E_{3p}^{(i)} - \varepsilon')}. \tag{A3}$$

The second CF $\phi_{\ell'}(r)$ is determined as

$$\phi_{\ell'}(r) = \sum_{\varepsilon'>F} \frac{P_{\varepsilon'\ell'}(r)[a_1\langle\varepsilon'\ell'|y_1(3p,\phi_{\ell''})|3p\rangle + b_2\langle\varepsilon'\ell'|y_2(3p,3p)|\phi_{\ell''}\rangle]}{(\omega - E^{(i)}_{3p} - \varepsilon')}. \tag{A4}$$

The $\phi_{\ell'}(r)$ CF is determined via solving the following inhomogeneous integrodifferential equation:

$$\begin{aligned}(h_{\ell'} - \omega + E^{(i)}_{3p})\phi_{\ell'}(r) = &-a_1\left[y_1(3p,\phi_{\ell''})P_{3p}(r) - \sum_{n'<F} P_{n'\ell'}(r)\langle n'\ell'|y_1(3p,\phi_{\ell''})|3p\rangle\right]\\ &-b_2\left[y_2(3p,3p)\phi_{\ell''}(r) - \sum_{n'<F} P_{n'\ell'}(r)\langle n'\ell'|y_2(3p,3p)|\phi_{\ell''}\rangle\right]\end{aligned} \tag{A5}$$

where $h_{\ell'}$ is the HF operator for the $\varepsilon'\ell'$ electron in the $3p^5\varepsilon'\ell'(^1P)$ configuration.

As a result, the expression for the transition amplitude (A1) becomes

$$t^{(\mathrm{II})}_{\omega}(L,\ell,\ell',\ell'') = \langle\varepsilon\ell|d|\phi_{\ell'}\rangle. \tag{A6}$$

2. Ground-state correlation processes (IIIa) and (IIIb)

Transition amplitudes for the processes (IIIa) and (IIIb), $T^{(\mathrm{corr})}_{q,\omega}$, have identical numerators but different energy denominators. After summation of those amplitudes and bringing the fractions to a common denominator the resulting expression for the radial part of the transition amplitude of two processes (IIIa) and (IIIb) $t^{(\mathrm{IIIa,b})}_{\omega}$ takes the form

$$t^{(\mathrm{IIIa,b})}_{\omega}(L,\ell,\ell',\ell'') = \sum_{\varepsilon',\varepsilon''>F} \frac{\langle\varepsilon\ell|d|\varepsilon'\ell'\rangle\langle 3p|d|\varepsilon''\ell''\rangle\sum_k c_k\langle\varepsilon'\ell'|y_k(\varepsilon''\ell'',3p)|3p\rangle}{(\omega - E^{(i)}_{3p} - \varepsilon')(E^{(i)}_{3p} - E^{(i)}_{3p^2} - \omega - \varepsilon'')}, \tag{A7}$$

where $E^{(i)}_{3p^2}$ is the double-ionization potential of the Ar $3p$ shell. The experimental ionization potential $E^{(i)}_{3p^2} = 3.189$ Ry was used in the calculation.

One should note that Eq. (A7) becomes identical to Eq. (23) from [14] if we assume $E^{(i)}_{3p^2} = 2E^{(i)}_{3p}$. Coefficients c_k entering Eq. (A7) were determined using the effective operators method [27,33]. They are tabulated in Table III.

The transition amplitude (A7) was calculated using two CFs. First, $\phi_{\ell''}$, is the solution of the following equations for the length and velocity form, respectively:

$$(h_{\ell''} + \omega + E^{(i)}_{3p^2} - E^{(i)}_{3p})\phi_{\ell''}(r) = -P_{3p}(r)\,r + \sum_{n''<F}\langle 3p|r|n''\ell''\rangle P_{n''\ell''}(r), \tag{A8}$$

$$(h_{\ell''} + \omega + E^{(i)}_{3p^2} - E^{(i)}_{3p})\phi_{\ell''}(r) = -\left(\frac{dP_{3p}(r)}{dr} \mp \frac{\ell_{\max}}{r}P_{3p}(r)\right) + \sum_{n''<F}\langle 3p|d|n''\ell''\rangle P_{n''\ell''}(r), \tag{A9}$$

where $h_{\ell''}$ is the HF operator for the $\varepsilon''\ell''$ electron in the $3p^5\varepsilon''\ell''(^1P)$ configuration.

According to the notes to Eq. (8) the sign + in the latter equation corresponds to the $\ell'' = 0$ case and − corresponds to the $\ell'' = 2$.

The second CF, $\phi_{\ell'}$, is the solution of the following equation:

$$(h_{\ell'} - \omega + E^{(i)}_{3p})\phi_{\ell'}(r) = -\sum_k c_k\left[y_k(\phi_{\ell''},3p)P_{3p}(r) - \sum_{n'<F} P_{n'\ell'}(r)\langle n'\ell'|y_k(\phi_{\ell''},3p)|3p\rangle\right], \tag{A10}$$

where $h_{\ell'}$ is the HF operator for the $\varepsilon'\ell'$ electron in the $3p^5\varepsilon'\ell'(^1P)$ configuration.

Finally, the expression for the transition amplitude (A7) is

$$t^{(\mathrm{IIIa,b})}_{\omega}(L,\ell,\ell',\ell'') = \langle\varepsilon\ell|d|\phi_{\ell'}\rangle. \tag{A11}$$

3. Ground-state correlation process (IIIc)

The radial part of the transition amplitude of this process is

$$t^{(\mathrm{IIIc})}_{\omega}(L,\ell,\ell',\ell'') = \sum_{\varepsilon',\varepsilon''>F} \frac{\langle 3p|d|\varepsilon'\ell'\rangle\langle\varepsilon'\ell'|d|\varepsilon''\ell''\rangle\sum_k c_k\langle\varepsilon''\ell''|y_k(\varepsilon\ell,3p)|3p\rangle}{(E^{(i)}_{3p} - E^{(i)}_{3p^2} - \omega - \varepsilon')(E^{(i)}_{3p} - E^{(i)}_{3p^2} - 2\omega - \varepsilon'')}. \tag{A12}$$

TABLE IV. The c_k coefficients entering Eq. (A12).

^1L	ℓ	ℓ'	ℓ''	c_0	c_2	c_4
^1S	p	s,d	p	5	$-\frac{2}{5}$	0
^1D	p	s,d	p	-1	$\frac{11}{25}$	0
^1D	p	d	f	0	$\frac{54}{25}$	0
^1D[a]	f	s	p	0	$\frac{1}{5}$	0
^1D	f	d	p	0	$\frac{1}{25}$	0
^1D	f	d	f	0	$\frac{123}{175}$	$-\frac{4}{21}$

[a]For this case the coefficients f_q in Eq. (18) should be taken from Table I for $\ell' = 2$.

The coefficients c_k entering Eq. (A12) cannot be derived using the effective operator technique: they turned out to be dependent on the total orbital angular momentum L of the final state. The expressions for the geometrical factors in the Coulomb and dipole matrix elements in the amplitude (A12) were derived applying the methods of [26]. The coefficients c_k, tabulated in Table IV, were obtained by summation of the product of those three expressions over the quantum numbers of intermediate states.

TABLE V. The c_k coefficients entering Eq. (A16).

^1L	ℓ	c_0	c_2
^1S	p	-5	$\frac{2}{5}$
^1D	p	1	$-\frac{11}{25}$
^1D	f	0	$-\frac{1}{5}$

To simplify Eq. (A12) the two CFs are defined: the $\phi_{\ell'}$ CF is the solution of Eqs. (A8) and (A9) rewritten for the $\phi_{\ell'}$ and the $\phi_{\ell''}$ is the solution of the following equation:

$$(h_{\ell''} + 2\omega + E^{(i)}_{3p^2} - E^{(i)}_{3p})\phi_{\ell''}(r) = -\sum_k c_k \left[y_k(\varepsilon\ell,3p)P_{3p}(r) - \sum_{n''<F} P_{n''\ell''}(r)\langle n''\ell''|y_k(\varepsilon\ell,3p)|3p\rangle \right], \tag{A13}$$

where $h_{\ell''}$ is the HF operator for the $\varepsilon''\ell''$ electron in the $3p^5\varepsilon''\ell''(^1P)$ configuration.

As a result, the amplitude (A12) becomes

$$t^{(\mathrm{IIIc})}_{\omega}(L,\ell,\ell',\ell'') = \langle\phi_{\ell'}|d|\phi_{\ell''}\rangle. \tag{A14}$$

4. Intermediate-state shake-up correlation process (IV)

In order to decouple the denominators in the expression of this correlation amplitude we took into account the orthonormality condition for the continuum states similar to work [14]:

$$\langle\varepsilon'\ell'|\varepsilon''\ell'\rangle = \delta(\varepsilon' - \varepsilon''). \tag{A15}$$

Then, the expression for the radial part of this transition amplitude becomes

$$t^{(\mathrm{IV})}_{\omega}(L,\ell,\ell') = \sum_{\varepsilon',\varepsilon''>F} \frac{\langle 3p|d|\varepsilon'\ell'\rangle\langle\varepsilon'\ell'|\varepsilon''\ell'\rangle\langle\varepsilon''\ell'|d|3p\rangle\sum_k c_k\langle\varepsilon\ell|y_k(3p,3p)|3p\rangle}{(E^{(i)}_{3p} - E^{(i)}_{3p^2} - \omega - \varepsilon')(\omega - E^{(i)}_{3p} - \varepsilon'')}. \tag{A16}$$

The geometrical factors c_k in the amplitude (A16) cannot be derived using the effective operator technique. They were obtained using the methods of [26] and are listed in Table V. One should note that they were found to be independent of the ℓ' quantum number. In the radial part (A16) the quantum number ℓ'' is absent. Therefore, in Eq. (18) the sum over the ℓ'' is also absent.

To compute the transition amplitude (A16) the two CFs were applied. The $\overline{\phi_{\ell'}}$ CF is the solution of differential equations (A8) and (A9) with replacing ℓ'' and $\phi_{\ell''}$ by ℓ' and $\overline{\phi_{\ell'}}$; the $\phi_{\ell'}$ CF is the solution of differential equations (10) and (11).

Finally, the expression for the transition amplitude (A16) takes the form

$$t^{(\mathrm{IV})}_{\omega}(L,\ell,\ell') = \langle\overline{\phi_{\ell'}}|\phi_{\ell'}\rangle\sum_k c_k R^k(\varepsilon\ell,3p;3p,3p). \tag{A17}$$

5. Intermediate-state electron-scattering correlation process (V)

The radial part of the correlation transition amplitude (V) is

$$t^{(\mathrm{V})}_{\omega}(L,\ell,\ell',\ell'') = \sum_{\varepsilon',\varepsilon''>F} \frac{\langle 3p|d|\varepsilon''\ell''\rangle\sum_k[a_k\langle\varepsilon''\ell''|y_k(\varepsilon\ell,\varepsilon'\ell')|3p\rangle + b_k\langle\varepsilon''\ell''|y_k(\varepsilon\ell,3p)|\varepsilon'\ell'\rangle]\langle\varepsilon'\ell'|d|3p\rangle}{(E^{(i)}_{3p} - E^{(i)}_{3p^2} - \omega - \varepsilon'')(\omega - E^{(i)}_{3p} - \varepsilon')}. \tag{A18}$$

The coefficients a_k and b_k entering Eq. (A18) were determined using the effective operator method and are tabulated in Table VI.

To compute the amplitude (A18) the CFs $\phi_{\ell'}$ were determined by solution of the differential equations (10) and (11). The CFs $\phi_{\ell''}$ were computed using Eqs. (A8) and (A9).

TABLE VI. The values of the a_k and b_k coefficients entering Eq. (A18).

ℓ	ℓ'	ℓ''	a_1	b_0	b_2	b_4
p	s	s	$\frac{2}{3}$	-1	0	0
p	s	d	$\frac{4}{3}$	0	$-\frac{2}{5}$	0
p	d	s	$\frac{2}{3}$	0	$-\frac{2}{5}$	0
p	d	d	$\frac{4}{3}$	-1	$-\frac{1}{5}$	0
f	d	s	$\frac{2}{3}$	0	$-\frac{1}{5}$	0
f	d	d	$\frac{4}{3}$	0	$-\frac{2}{35}$	$-\frac{4}{21}$

Since the CFs $\phi_{\ell'}$ and $\phi_{\ell''}$ were determined the transition amplitude (A18) became

$$t_\omega^{(\mathrm{V})}(L,\ell,\ell',\ell'') = \sum_k [a_k R^k(\phi_{\ell''},\varepsilon\ell;3p,\phi_{\ell'}) + b_k R^k(\phi_{\ell''},\varepsilon\ell;\phi_{\ell'},3p)]. \quad \text{(A19)}$$

6. Final-state electron-scattering correlation processes (VIa) and (VIb)

Similar to the cases (IIIa) and (IIIb) transition amplitudes of the processes (VIa) and (VIb) have identical numerators. Their sum is expressed by Eq. (18) where the radial part of the amplitude is

$$\begin{aligned} t_\omega^{(\mathrm{VIa,b})}(L,\ell,\ell',\ell'') &= \sum_{\varepsilon',\varepsilon''>F} \sum_k [a_k \langle\varepsilon\ell|y_k(3p,\varepsilon''\ell'')|\varepsilon'\ell'\rangle \\ &\quad + b_k \langle\varepsilon\ell|y_k(3p,\varepsilon'\ell')|\varepsilon''\ell''\rangle]\langle\varepsilon''\ell''|d|3p\rangle\langle\varepsilon'\ell'|d|3p\rangle \\ &\quad \times \left\{ \frac{1}{(2\omega - E_{3p^2}^{(i)} - \varepsilon' - \varepsilon'')(\omega - E_{3p}^{(i)} - \varepsilon')} \right. \\ &\quad \left. + \frac{1}{(2\omega - E_{3p^2}^{(i)} - \varepsilon' - \varepsilon'')(\omega - E_{3p}^{(i)} - \varepsilon'')} \right\}. \end{aligned} \quad \text{(A20)}$$

Coefficients a_k and b_k entering Eq. (A20) were determined using the effective operator method and are tabulated in Table VII.

The first factor in the denominator of terms standing in the curly braces of Eq. (A20) contains both the ε' and ε'' intermediate state energies. Therefore, the amplitude (A20) cannot be expressed via CFs.

In Ref. [14] in the calculation of the sum of two amplitudes (VIa) and (VIb) the experimental double-ionization potential $E_{3p^2}^{(i)}$ of Ar was used. In this case, in order to apply the implicit functions obtained by the variationally stable procedures method, the authors employed an additional approximation in Eq. (A20): in the first factor of the first fraction in curly braces, containing 2ω, they offered $\varepsilon' = \varepsilon''$ and in the first factor of the second fraction in curly braces, containing 2ω, they took $\varepsilon'' = \varepsilon'$. After this assumption the expression for the transition amplitude (A20) became

TABLE VII. The a_k and b_k coefficients entering Eq. (A20).

ℓ	ℓ'	ℓ''	a_1	b_1	b_3
p	s	s	$\frac{2}{3}$	$-\frac{1}{3}$	0
p	s	d	$\frac{4}{3}$	$-\frac{2}{3}$	0
p	d	s	$\frac{2}{3}$	$-\frac{1}{3}$	0
p	d	d	$\frac{4}{3}$	$-\frac{1}{15}$	$-\frac{9}{35}$
f	d	s	$\frac{2}{3}$	0	$-\frac{1}{7}$
f	d	d	$\frac{4}{3}$	$-\frac{2}{5}$	$-\frac{4}{35}$

$$\begin{aligned} t_\omega^{(\mathrm{VIa,b})}(L,\ell,\ell',\ell'') &= \sum_{\varepsilon',\varepsilon''>F} \sum_k [a_k \langle\varepsilon\ell|y_k(3p,\varepsilon''\ell'')|\varepsilon'\ell'\rangle \\ &\quad + b_k \langle\varepsilon\ell|y_k(3p,\varepsilon'\ell')|\varepsilon''\ell''\rangle]\langle\varepsilon''\ell''|d|3p\rangle\langle\varepsilon'\ell'|d|3p\rangle \\ &\quad \times \frac{1}{2}\left\{ \frac{1}{(\omega - 0.5E_{3p^2}^{(i)} - \varepsilon'')(\omega - E_{3p}^{(i)} - \varepsilon')} \right. \\ &\quad \left. + \frac{1}{(\omega - 0.5E_{3p^2}^{(i)} - \varepsilon')(\omega - E_{3p}^{(i)} - \varepsilon'')} \right\}. \end{aligned} \quad \text{(A21)}$$

In the calculation of transition amplitudes via Eq. (A21) the four CFs, $\phi_{\ell'},\overline{\phi_{\ell''}}$ and $\overline{\phi_{\ell'}},\phi_{\ell''}$ were applied. CFs $\phi_{\ell'},\overline{\phi_{\ell''}}$ are used for computing the first term in curly braces and CFs $\overline{\phi_{\ell'}},\phi_{\ell''}$ for the second one. The $\phi_{\ell'}$ and $\phi_{\ell''}$ CFs are the solutions of the inhomogeneous equations (10) and (11), whereas $\overline{\phi_{\ell'}}$ and $\overline{\phi_{\ell''}}$ are the solutions of the same equations with $E_{3p}^{(i)}$ replaced by $0.5E_{3p^2}^{(i)}$. Finally, the transition amplitude (A21) is

$$\begin{aligned} t_\omega^{(\mathrm{VIa,b})}(L,\ell,\ell',\ell'') &= \frac{1}{2}\sum_k \{a_k[R^k(\varepsilon\ell,3p;\phi_{\ell'},\overline{\phi_{\ell''}}) + R^k(\varepsilon\ell,3p;\overline{\phi_{\ell'}},\phi_{\ell''})] \\ &\quad + b_k[R^k(\varepsilon\ell,3p;\overline{\phi_{\ell''}},\phi_{\ell'}) + R^k(\varepsilon\ell,3p;\phi_{\ell''},\overline{\phi_{\ell'}})]\}. \end{aligned} \quad \text{(A22)}$$

Another approximation stems from the supposition $E_{3p^2}^{(i)} = 2E_{3p}^{(i)}$. In this case two terms in the curly braces of (A20) can be summed. The result is

$$t_\omega^{(\mathrm{VIa,b})}(L,\ell,\ell',\ell'') = \sum_{\varepsilon',\varepsilon''>F} \frac{\sum_k [a_k \langle\varepsilon\ell|y_k(3p,\varepsilon''\ell'')|\varepsilon'\ell'\rangle + b_k \langle\varepsilon\ell|y_k(3p,\varepsilon'\ell')|\varepsilon''\ell''\rangle]\langle\varepsilon''\ell''|d|3p\rangle\langle\varepsilon'\ell'|d|3p\rangle}{(\omega - E_{3p}^{(i)} - \varepsilon'')(\omega - E_{3p}^{(i)} - \varepsilon')}. \quad \text{(A23)}$$

TABLE VIII. Summed amplitudes of the processes (VIa) and (VIb) for the transition to the $\varepsilon p(^1D)$ channel calculated in different approximation at $\omega = 8$ eV (in 10^{-25} cm^2 s$^{1/2}$).

Approx.	Length	Velocity
Eq. (A20)[a]	−0.1440	−0.4826
Eq. (A21)[a]	−0.1340	−0.4455
Eq. (A21)[b]	−0.1345	−0.4470
Eq. (A23)[a]	−0.2388	−0.7699
Eq. (A23)[b]	−0.2399	−0.7731

[a]Method of direct integration.
[b]Method of correlation function.

In this case both CFs $\phi_{\ell'}$ and $\phi_{\ell''}$ have the same expression (9) and are the solutions of the same inhomogeneous equation (10) or (11) for the length or velocity form, respectively. Finally, the transition amplitude (A23) is

$$t_\omega^{(\mathrm{VIa,b})}(L,\ell,\ell',\ell'') = \sum_k [a_k R^k(\varepsilon\ell,3p;\phi_{\ell'},\phi_{\ell''}) + b_k R^k(\varepsilon\ell,3p;\phi_{\ell''},\phi_{\ell'})]. \quad \text{(A24)}$$

In the present paper we investigated the inaccuracy caused by replacing the exact expression (A20) by (A21) or (A23). For this purpose the radial part of the transition amplitude (A20) to the $3p^5\varepsilon p(^1D)$ channel was calculated using the direct integration method as it was made in Ref. [12]. Similar to that work, the cutoff $R_{\max} = 20.365$ a.u. was applied and the basis set of $\varepsilon'\ell'$ and $\varepsilon''\ell''$ functions computed in the $3p^5(\varepsilon'\ell'/\varepsilon''\ell'')(^1P)$ configuration contained 6 discrete and 56 continuum wave functions in the 0–24.6-Ry energy range.

The results of the calculation at the near-threshold energy $\omega = 8$ eV are tabulated in Table VIII and compared with the approximated data discussed above. Comparison of the data of line 2 with line 3 as well as line 4 with line 5 affirms a good accuracy of the direct integration method in the near-threshold region: the difference of the method does not exceed 0.5% for both length and velocity forms. Therefore, the results listed in the first line can be treated as a reliable one. From the comparison of the data of first, second, and fourth lines it is obvious that the expression (A21) provides better agreement to the exact values from (A20) than the approximation (A23). In the first case the error is 7–8% only whereas in the second case it rises up to 60–70%.

Based on this study, we calculated the summed amplitude of the processes (VIa) and (VIb) applying Eq. (A21). The question may arise of why we did not use the method of direct integration in the calculation of the radial transition amplitude (A20) in the whole photon energy range. The reason is that this method becomes unstable and less reliable at the photon energies $\omega > 12$ eV, as it was noted in the paper [12].

[1] W. Ackermann, G. Asova, V. Ayvazyan *et al.*, Operation of a free-electron laser from the extreme ultraviolet to the water window, Nat. Photon. **1**, 336 (2007).

[2] T. Ishikawa, H. Aoyagi, T. Asaka *et al.*, A compact x-ray free-electron laser emitting in the sub-angström region, Nat. Photon. **6**, 540 (2012).

[3] M. G. Makris and P. Lambropoulos, Reexamination of multiphoton ionization of xenon under 12.7-ev radiation, Phys. Rev. A **77**, 023415 (2008).

[4] M. G. Makris and P. Lambropoulos, Theoretical interpretation of multiphoton ionization of neon by soft-x-ray intense radiation, Phys. Rev. A **77**, 023401 (2008).

[5] M. G. Makris, P. Lambropoulos, and A. Mihelič, Theory of Multiphoton Multielectron Ionization of Xenon Under Strong 93-eV Radiation, Phys. Rev. Lett. **102**, 033002 (2009).

[6] P. Lambropoulos, K. G. Papamihail, and P. Decleva, Theory of multiple ionization of xenon under strong xuv radiation and the role of the giant resonance, J. Phys. B: At. Mol. Opt. Phys. **44**, 175402 (2011).

[7] R. Santra and C. H. Greene, Multiphoton ionization of xenon in the vuv regime, Phys. Rev. A **70**, 053401 (2004).

[8] H. Fukuzawa, S.-K. Son, K. Motomura *et al.*, Deep Inner-Shell Multiphoton Ionization by Intense X-Ray Free-Electron Laser Pulses, Phys. Rev. Lett. **110**, 173005 (2013).

[9] S.-K. Son, L. Young, and R. Santra, Impact of hollow-atom formation on coherent x-ray scattering at high intensity, Phys. Rev. A **83**, 033402 (2011).

[10] L.-W. Pi and A. F. Starace, Potential barrier effects in two-photon ionization processes, Phys. Rev. A **82**, 053414 (2010).

[11] X. Tang, T. N. Chang, P. Lambropoulos, S. Fournier, and L. F. DiMauro, Multiphoton ionization of magnesium with configuration-interaction calculations, Phys. Rev. A **41**, 5265 (1990).

[12] M. S. Pindzola and H. P. Kelly, Two-photon ionization of the neutral argon atom, Phys. Rev. A **11**, 1543 (1975).

[13] A. F. Starace and T.-F. Jiang, Transition-matrix theory for two-photon ionization of rare-gas atoms and isoelectronic ions with application to argon, Phys. Rev. A **36**, 1705 (1987).

[14] C. Pan, B. Gao, and A. F. Starace, Two-photon ionization of the ar atom and detachment of the f$^-$ ion, Phys. Rev. A **41**, 6271 (1990).

[15] C. Pan and A. F. Starace, Angular distribution of electrons following two-photon ionization of the ar atom and two-photon detachment of the f$^-$ ion, Phys. Rev. A **44**, 324 (1991).

[16] A. Dalgarno and J. Lewis, The exact calculation of long-range forces between atoms by perturbation theory, Proc. R. Soc. London **233**, 70 (1955).

[17] R. Sternheimer, On nuclear quadrupole moments, Phys. Rev. **84**, 244 (1951).

[18] J. C. Morrison, Effect of core polarization upon the $f-f$ interactions of rare-earth and actinide ions, Phys. Rev. A **6**, 643 (1972).

[19] T. Chang, Influence of electronic correlation effects on the photoionization of sodium and potassium, J. Phys. B: At. Mol. Phys. **8**, 743 (1975).

[20] V. L. Sukhorukov, B. M. Lagutin, I. D. Petrov, H. Schmoranzer, A. Ehresmann, and K.-H. Schartner, Photoionization of Kr near 4s threshold. II. Intermediate-coupling theory, J. Phys. B: At. Mol. Opt. Phys. **27**, 241 (1994).

[21] T. N. Chang and R. T. Poe, Calculation of multiphoton ionization processes, J. Phys. B: At. Mol. Phys. **9**, L311 (1976).

[22] T. N. Chang and R. T. Poe, Two- and three-photon ionization of hydrogen and lithium, Phys. Rev. A **16**, 606 (1977).

[23] K. Smith, R. J. W. Henry, and P. G. Burke, Scattering of electrons by atomic systems with configurations $2p^q$ and $3p^q$, Phys. Rev. **147**, 21 (1966).

[24] P. V. Demekhin, B. M. Lagutin, and I. D. Petrov, Theoretical study of angular-resolved two-photon ionization of H_2, Phys. Rev. A **85**, 023416 (2012).

[25] I. D. Petrov, V. L. Sukhorukov, and H. Hotop, The influence of core polarization on photo-ionization of alkali and metastable rare gas atoms near threshold, J. Phys. B: At. Mol. Opt. Phys. **32**, 973 (1999).

[26] A. P. Jucys and A. J. Savukinas, *Mathematical Foundation of the Atomic Theory*, 1st ed. (Mintis, Vilnius, 1973) (in Russian).

[27] I. Lindgren and J. Morrison, *Atomic Many-body Theory*, Chemical Physics Vol. 13 (Springer-Verlag, Berlin, 1982).

[28] L. Minnhagen, The spectrum of singly ionized argon, Ar II, Ark. Fys. **25**, 203 (1963).

[29] A. Hibbert and J. Hansen, Accurate wavefunctions for 2 s and 2 p 0 states in ar ii, J. Phys. B: At. Mol. Phys. **20**, L245 (1987).

[30] A. Kramida, Y. Ralchenko, J. Reader, and N. Team, *NIST Atomic Spectra Database (version 5.2)[Online]* (Physics Laboratory of NIST, 2014) http://physics.nist.gov/PhysRefData/ASD/Html/verhist.shtml.

[31] H. Schmoranzer, A. Ehresmann, F. Vollweiler, V. L. Sukhorukov, B. M. Lagutin, I. D. Petrov, K.-H. Schartner, and B. Möbus, Photoionization of Kr near the 4s threshold. I. Experiment and LS coupling theory, J. Phys. B: At. Mol. Opt. Phys. **26**, 2795 (1993).

[32] P. Lambropoulos, Theory of multiphoton ionization: Near-resonance effects in two-photon ionization, Phys. Rev. A **9**, 1992 (1974).

[33] B. R. Judd, *Second Quantization and Atomic Spectroscopy* (John Hopkins, Baltimore, 1967).